Scientific accomplishments
Results obtained during the reporting period.

A. <u>Pulsed Laser induced transfer of hemp stalk biocomposite components as nano-composite structured thin films</u>

(Published as: Cocean, A.; Cocean, G.; Diaconu, M.; Garofalide, S.; Husanu, F.; Munteanu, B.S.; Cimpoesu, N.; Motrescu, I.; Puiu, I.; Postolachi, C.; Cocean, I. and Gurlui, S. Nano-Biocomposite Materials Obtained from Laser Ablation of Hemp Stalks for Medical Applications and Potential Component in New Solar Cells. Int. J. Mol. Sci. 2023, 24, 3892. https://doi.org/10.3390/ijms24043892

The studies that have been previously reported on pulsed laser interactions with natural polymers [1-3] and the effects induced by impurities in the laser ablation of silver target [4,5] provided information that allowed development of new studies to investigate behavior of biocomposites and the effect of inorganic atoms on the laser ablation process. Thus, the research of laser effects on polymeric biocomposites has continued with a study published in 2023 [6,7]. Pulsed laser deposition performed with YG 981E/IR-10 laser system, 532 nm laser beam of 300 μm radius was used with a pulse width of 10 ns, 10 Hz repetition rate and 150 mJ/pulse for 30 minutes using crushed hemp stalk (Figure 1 a) as laser ablated target resulted in a transfer of all of the biocomposite components in the thin film produced [6].

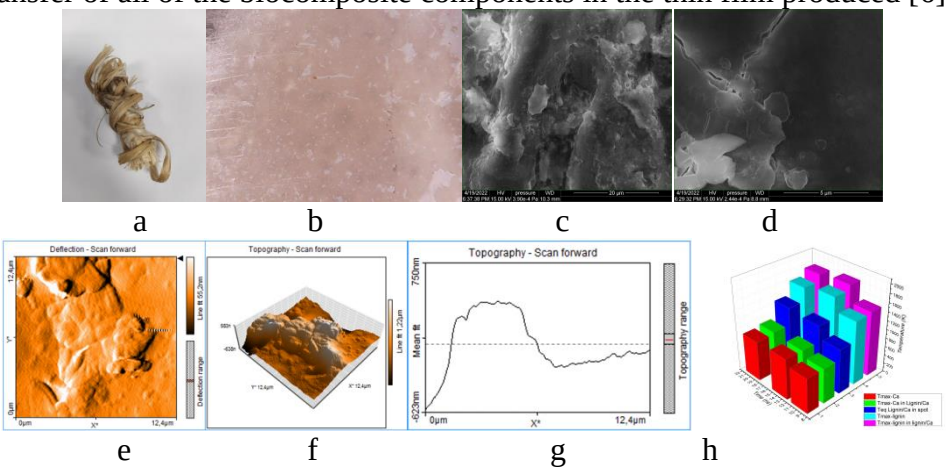

Figure 2.1. Target of crushed hemp stalk (a); microscope image of thin film obtained on glass slab (b); SEM image on hemp stalk and SEM image of the thin film (d); AFM 2D (e), 3D (f) and 1 D (g) topographic analysis; COMSOL simulation results on temperatures achieved during pulsed laser irradiation of hemp stalk (h)

The aspect of the thin film deposited on glass slab is translucent and of similar color to the hemp stalk target (Figure 1 a, b). Nano and aggregated structures were measured based on SEM (Scanning Electron Microscopy) and AFM (Atomic Force Microscopy) images using the soft Toup View.

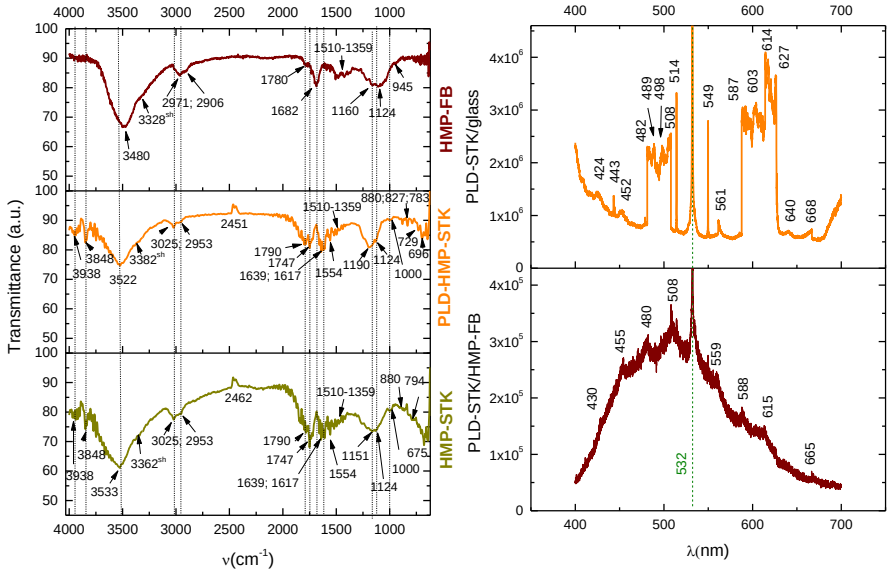

a b

Vibration Bands [cm⁻¹] HMP-STK	PLD-HMP-STK	HMP-FB	Functional Groups and References	Observations
3938	3938	-	O-H st free and bonded in phenols [29] O-H in adsorbed/absorbed water or in Mg-OH; Ca-OH [30]	lignin*p*-coumaric and ferulic acids (phenolic acids of parenchyma provenience)Mg-OHCa-OHAdsorbed water
3848	3848	-	O-H st free in alcohols [28] O-H in carboxylic acid, known to be typical carbohydrates [31]O-H in adsorbed/absorbed water or in Mg-OH; Ca-OH [30,32]	cellulose, hemicellulosestarch sugarsMg-OHCa-OHadsorbed water
3533 3362	3522 3382	3480 3328	O-H st intermolecular bonded in alcohols and phenols in polymers [5,21]O-H st in carboxylic acids [22,28,33]	cellulose, hemicellulose,starch,sugars,lignin*p*-coumaric and ferulic acids
3025	3025	-	Aryl C-H groups [1,28]	lignin*p*-coumaric and ferulic acids
2953	2953	2971 2906	Alkyl C-H groups [8,21,28,32]2971 cm⁻¹-possible Aryl C-H in lignin [7]	cellulose, hemicellulosestarch sugarsPossible lignin
2462	2451	-	O=C=O st (carbon dioxide) [28,32]	adsorbed CO2
1790	1790	1780	C=O st in carboxyl groups in conjugated acids and aldehydes, esters [5,23,28] C=O st in vinyl/phenyl ester [5,28]	ligninpectin*p*-coumaric and ferulic acidswaxes
1747	1747	-	C=O st in esters; [5,28] C=O st in carboxyl groups in conjugated acids of **parenchyma**and aldehydes, esters (in **pectin, lignin, wax**) [Ernö Pretch]Adsorbed formaldehyde [28,32]	waxes*p*-coumaric and ferulic acidspectinligninadsorbed formaldehyde
-	-	1682	C=O in carboxyl groups in carboxylic acids [8,28];C=O in conjugated aldehide or ketone [28]	*p*-coumaric and ferulic acids
1639	1639	-	O-H of adsorbed water [5];C=C st in monosubstituted alkene [28]	adsorbed water*p*-coumaric and ferulic acids
-	-	1617	C=C st in α,β-**unsaturated ketone**[28]	
1554	1554	-	Adsorbed formaldehyde [28]C=O in carboxyl groups [4,21,28,32,33]	adsorbed formaldehyde*p*-coumaric and ferulic acids
1510	1510	1510	C=C aromatic symetrical st [4,5,28]	lignin
1359	1359	1359	C-H bending [28];methoxyphenolic substitution in the aromatic ring [8,28];H in-plane bending in phenols in **lignin**[28]O-H in-plane bending, intermolecular bonded in alcohols in polymers [5,28]	cellulose, hemicellulosestarch sugarslignin
1151	1190	1160	Skeletal vibrations due to C-O-C asymmetric st in the oxane ring (cyclic ethers) [4,21,28]	cellulose (amorphous to crystalline 1160; 1190)HemicelluloseStarchpectin
1124	1124	1124	Skeletal vibrations due to C-O-C asymmetric st in the oxane ring (cyclic ethers) [21,28]	cellulose (amorphous to crystalline 1160; 1190)HemicelluloseStarchpectin
1000	1000	945	Skeletal vibrations due to C-O-C asymmetric st in the oxane ring (cyclic ethers) [28]Side groups vibrations [4,28]C=C bending in alkene in the carboxylic acids [28]	celluloseHemicelluloseStarchPectin*p*-coumaric and ferulic acids
880	880	-	Skeletal vibrations due to C-O-C symmetric st, C-C-O and C-C-H bendings [4,5,21,28];C=C bending in alkene in the carboxylic acids [28]	celluloseHemicelluloseStarchPectin*p*-coumaric and ferulic acids
-	827	-	C=C bending in alkene trisubstituted [28]	*p*-coumaric and ferulic acids
794	783	-	Out-of-plane bending in alkene in the carboxylic acids [28]	*p*-coumaric and ferulic acids
729	729	729	CH_2rocking [28];C=C bending in alkene disubstituted (cis) in the carboxylic acids [28]O-H out-of-plane bending [28]C-H bending [28]	Cellulose*p*-coumaric and ferulic acids
675	696	-	C-H bending and ring bending [28];C=C bending in alkene disubstituted (cis) in the carboxylic acids [28] C–H aromatic bending-out-of-plane modes [32]Adsorbed molecular CO_2[32]O-H out-of-plane bending [28];C-OH out-of-plane bending [5,28]	cellulose crystalline state,hemicellulose,starch,sugars,lignin*p*-coumaric and ferulic acidsadsorbed CO2
650–624	650–624	650–624	O-H out-of-plane bending [28]C-OH out-of-plane bending [5,28]	cellulose,hemicellulose,starch,sugars,lignin*p*-coumaric and ferulic acidsadsorbed water

c

Fluorecence [nm] PLD-HMP-STK/HMP-FB	PLD-HMP-STK/Glass	Emission, Fluorophores and References
430	424	Violet-blue due to *p*- coumaric acid and its derivatives [36,37]; bathochromic shift on PLD-HMP-STK/Glass
-	443	Blue due to coumaric acid derivatives [36,37]
455	452	Blue due to coumaric acid [36,37]; bathochromic shift on PLD-HMP-STK/Glass
480	482 v. strong	Blue-green due to ferulic acid [38,39]; slight hypsochromic shift
.498	489 v. strong	Blue-green due to ferulic acid [38,39]; bathochromic shift and enhanced intensity due to the *p*-coumaric acid concentration [38] on PLD-HMP-STK/Glass
508 (max)	508 v. strong	Green; enhanced fluorescence intensity on PLD-HMP-STK/Glass
-	549	Green-yellow
559	561	Yellow-green; hypsochromic shift and enhanced fluorescence intensity on PLD-HMP-STK/Glass
588	587 v. strong	Yellow; slight hypsochromic shift and enhanced fluorescence intensity on PLD-HMP-STK/Glass
-	603 v. strong	Yellow-red; assigned to chlorophyll [38]
615	614 v. strong	Yellow-red; slight hypsochromic shift and enhanced fluorescence intensity on PLD-HMP-STK/Glass
-	627 v. strong	Red-yellow; assigned to chlorophyll [38]
-	640	Red-yellow
665	668	Red; slight hypsochromic shift and enhanced fluorescence intensity on PLD-HMP-STK/Glass

d

Figure 2.2. FTIR spectra (a), LIF spectra (b) and results interpretation of functional groups in FTIR analysis (c) and fluorophores emission in LIF analysis (d)

The analyzes proved identical chemical composition re-organized in a nano-structured composite in the obtained thin films (Figure 2.2. a, c). The main chemical components are polymers (cellulose, lignin, hemicellulose, waxes, starch) and phenolic acids (p-coumaric and ferulic acids) as per Fourier Transform Infrared spectroscopy (FTIR) analysis (Figure 2.2. a and c). Laser Induced Fluorescence Spectroscopy

(LIF) evidenced emissions specific to the fluorophores of coumaric and ferulic acids and also to chlorophyll.
The EDX (Energy Dispersive X-ray Spectroscopy) shows and increase in calcium and magnesium concentration from an average of 1.5% calcium and 0.2% magnesium in the HMP-STK target to an average of 2.2% calcium and 1.2% magnesium in the PLD-HMP-STK thin films, while carbon content decreased from an average of 66% in HMP-STK target to 50% or less in the PLD-HMP-STK thin films. The results of the simulation in COMSOL of the pulsed laser irradiation, as plots of maximum temperatures achieved due to laser beam absorption and heat diffusion by calcium and lignin (Tmax-Ca and Tmax-lignin) compared to calcium and lignin as components in the lignin/Ca composite (Tmax-Ca in lignin/Ca and Tmax-lignin in lignin/Ca) and at an equilibrium in the spot center of the composite (Teq lignin/Ca in spot) are presented in Figure 2.1. h. The simulation provides information on the heating enhancement processes on both lignin and calcium; this could explain the increase in calcium content in the PLD-HMP-STK compared to the HMP-STK target.
The thin film obtained from hemp stalk proves good tribological properties. A large domain of functional applications is suitable for the nano-biocomposite thin film fabricated from hemp stalk by PLD from medicine (in transdermal drug delivery devices - TDD systems; gas sensing in medicine) to solar cells and also as medium for metallic impurities for further transfer of metals by laser irradiation and for the study of other intensified transfer and kinetic processes.

B. Study of optimization of polymeric matrix for controlling silver particles laser ablation and accelerated kinetic

The influence of the target impurities on the laser ablation that have already been reported [1-7] proved the role of heating characteristics of the impurity materials and/or of the matrix material to replace the optical characteristics unfavorable to the absorption of laser radiation in the laser ablation process. In the new study reported herein, three target samples with metallic filers in a polymeric composite were fabricated and their interactions with the pulsed laser beam were compared to a reference target sample.

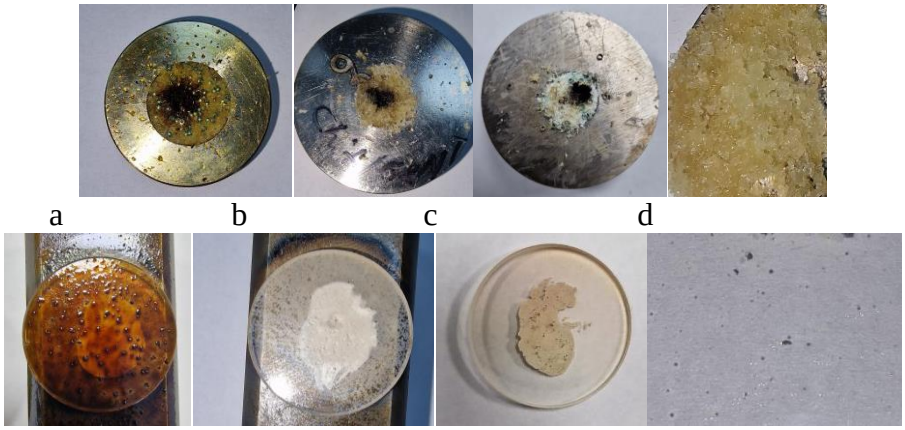

Figure 2.3. The target samples Chit-Oil-AgP (a); Chit-Oil-GRNT (b); Chit-AcC-AgP (c); Chit-Oil (d) and the resulted PLD thin films Chit-Oil-AgP-PLD (e); Chit-Oil-GRNT-PLD (f); Chit-AcC-AgP-PLD (g); Chit-Oil-PLD (h)

The targets with metallic insertion were fabricated as it follows: 1. chitosan mixed with flax oil and particles of silver (Chit-Oil-AgP) were included in the mixture; 2. chitosan mixed with flax oil and a garnet gemstone (Chit-Oil-GRNT) of grain size was included in the middle of the target; 3. chitosan mixed with citric acid aqueous solution and particles of silver (Chit-AcC-AgP), the mixture being treated with sodium bicarbonate. The reference sample was fabricated from chitosan mixed with flax oil (Chit-Oil). The reference sample was placed on a silver disk.

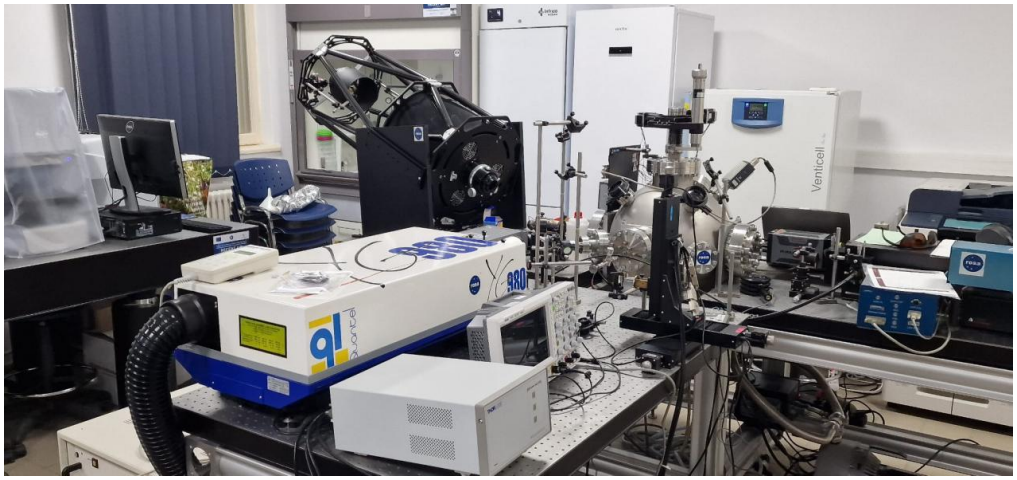

a

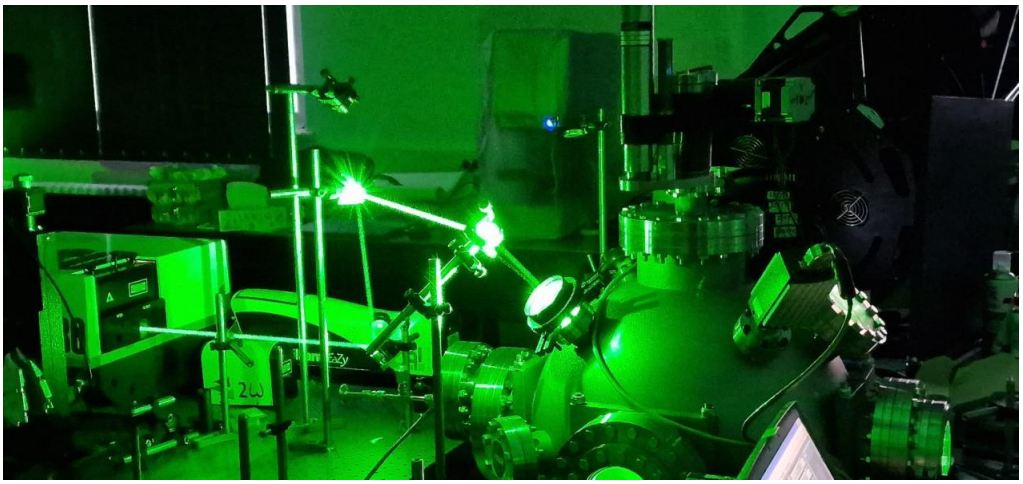

b

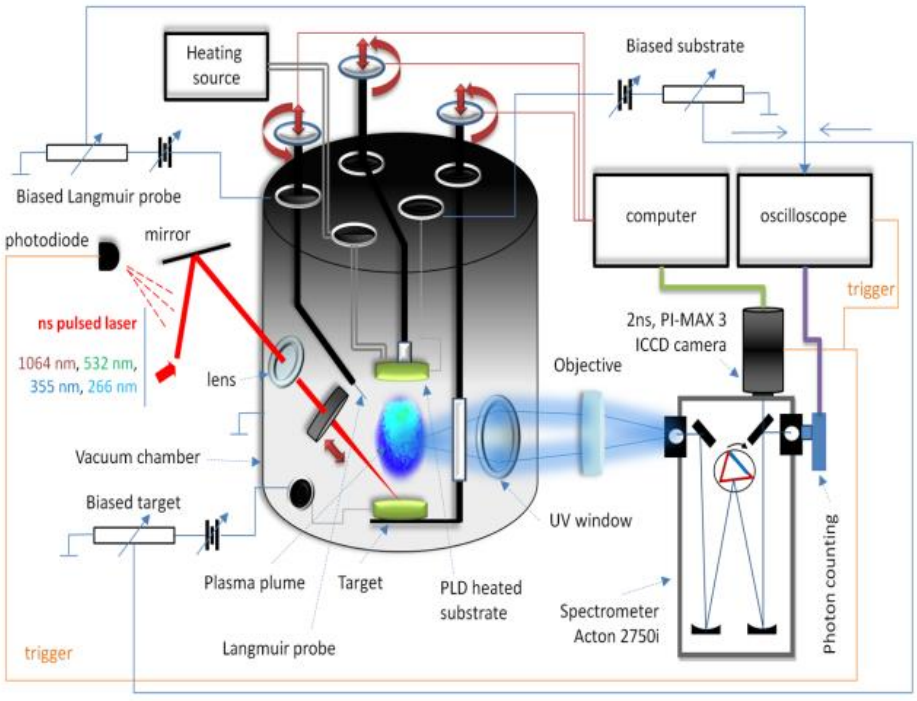

c

Figure 2.4. Laser installation with YG 981E/IR-10 laser system - Quantel, Les Ulis, France- set-up at LOASL (a) and (b) and its schematic representation (c)

Each sample was used as target in PLD processes performed with the YG 981E/IR-10 laser system, 532 nm laser beam of 650 μm radius was used with a pulse width of 10 ns, 10 Hz repetition rate and 60 mJ/pulse for 30 minutes.

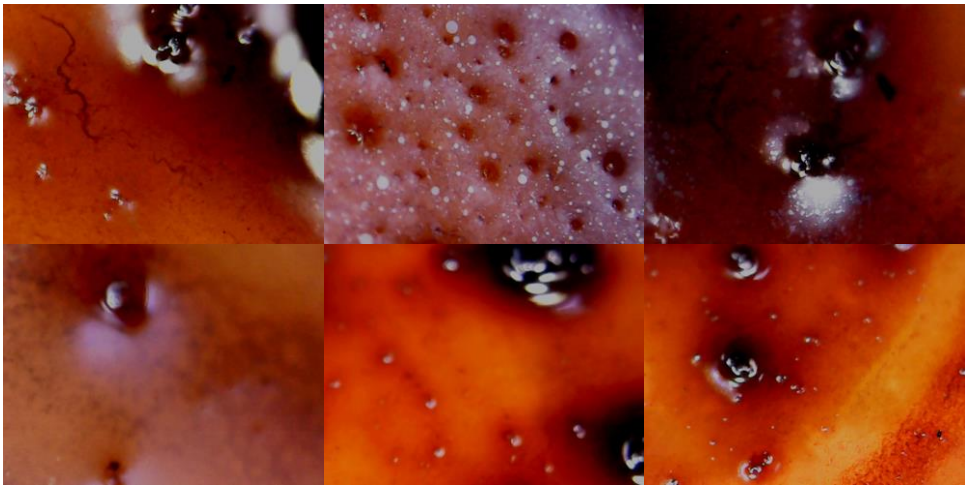

a

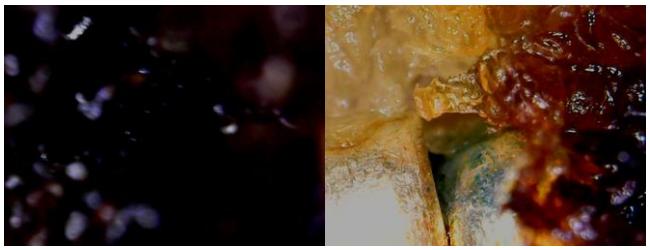

b

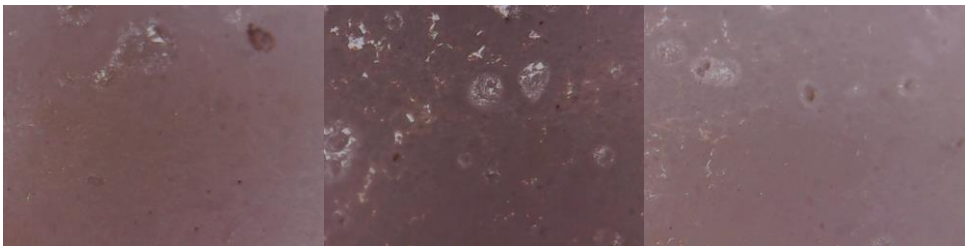

c

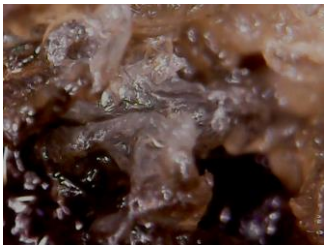

d

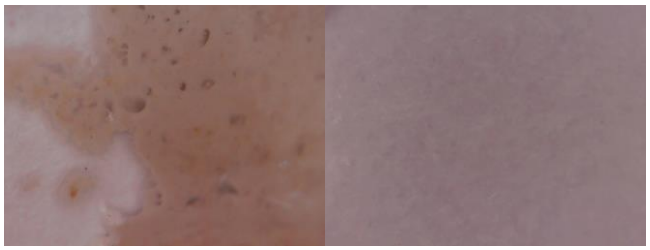

e

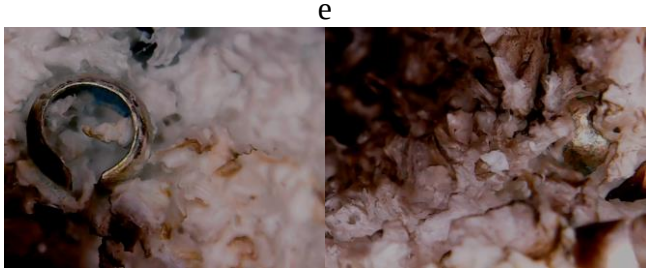

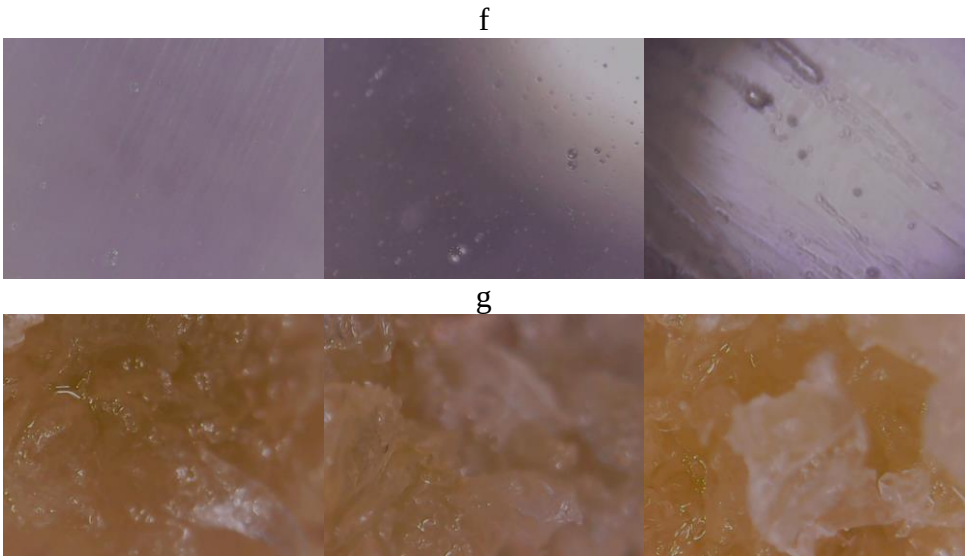

Figure 2.5. Microscope images of Chit-oil-AgP-PLD (a); Chit-oil-AgP target ablated (b); Chit-oil-GRNT-PLD (c); Chit-oil-GRNT target ablated (d); Chit-AcC-AgP-PLD (e); Chit-AcC-AgP target (f); Chit-oil-PLD (g); Chit-oil target ablated (h)

Microscope images in Figure 2.5 (a-h) show the laser irradiation effects on each of the four tested samples. The highest yield of ablated material was obtained from the Chit-Oil-AgP target, noticed as preponderantly oil with visible thermal effects on the target irradiated spot. Thin films were obtained from Chit-Oil-GRNT, and Chit-AcC-AgP , induced thermal effects being also well observed. The reference sample Chit-Oil almost has not been ablated.

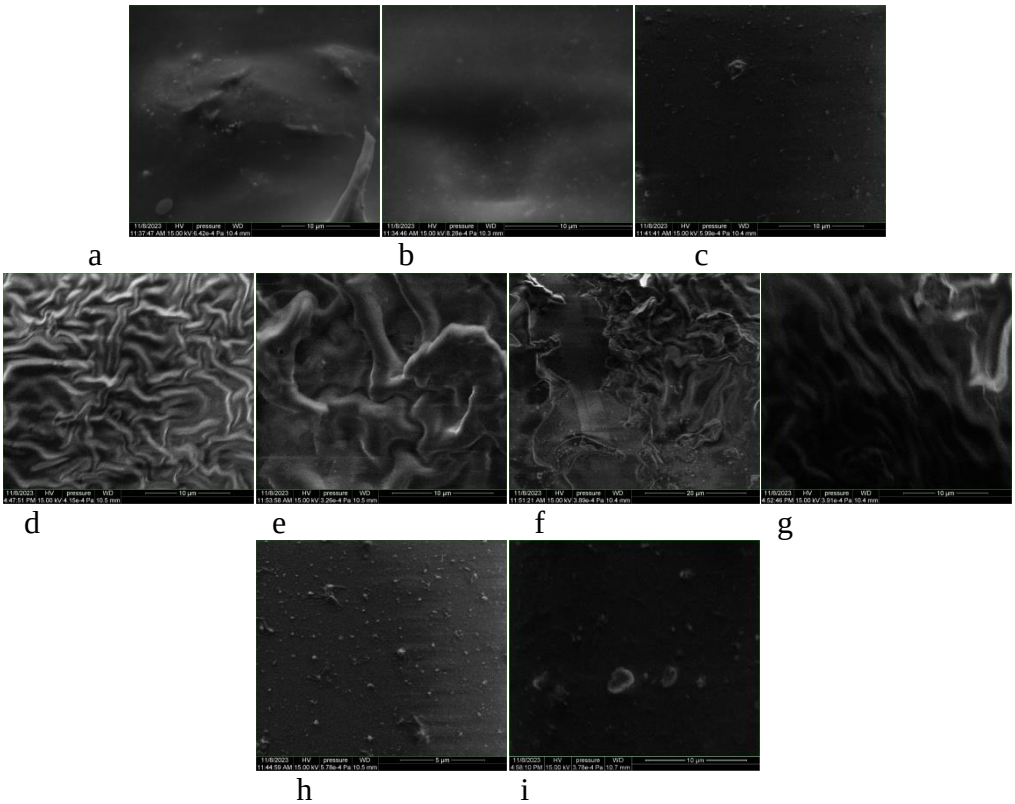

Figure 2.6. SEM images of the thin films Chit-Oil-AgP-PLD (a), (b), (c); Chit-Oil-GRNT-PLD (d), (e), (f), (g); Chit-AcC-AgP-PLD (h), (i)

The thin films resulted in particular morphological structures (Figure 2.6). Comparing images in Figure 2.6 for Chit-Oil-AgP-PLD (a), (b), (c) to the images for Chit-Oil-GRNT-PLD (d), (e), (f), (g), where the

composite matrix is the same (chitosan and flax oil) and the impurities or "immersed" material is different, a first conclusion is that silver particles favored abundant oil ablation, while the garnet favored ablation of the solid material, mainly chitosan.

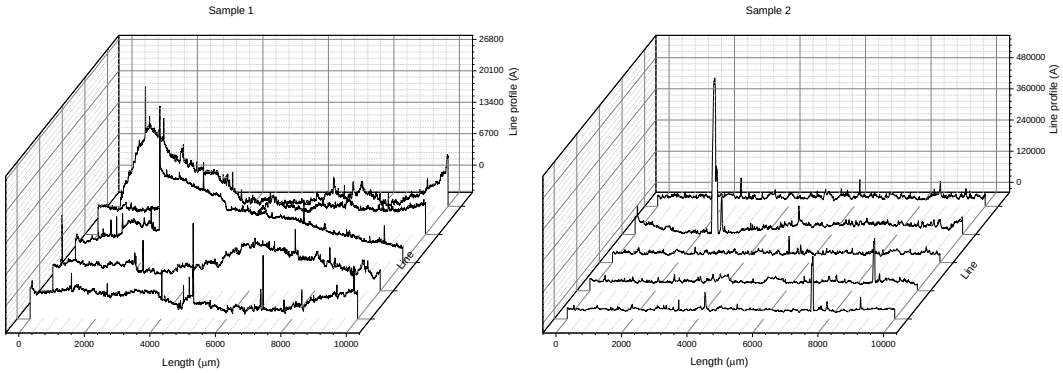

Figure 2.7. Profilometry performed on the thin films Chit-AcC-AgP-PLD sample 1 (a) and Chit-Oil-GRNT-PLD sample 2 (b)

The thin film topography performed with DektakXT Profilometer Bruker on the Chit-Oil-GRNT and Chit-AcC-AgP-PLD is in accordance with the 2 D SEM images pattern.

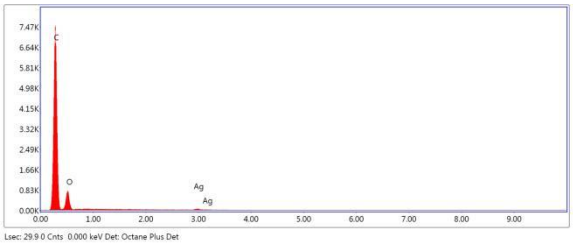

a

Element	Weight %	Atomic %
C K	74.58	79.76
O K	25.18	20.22
AgL	0.24	0.03

b

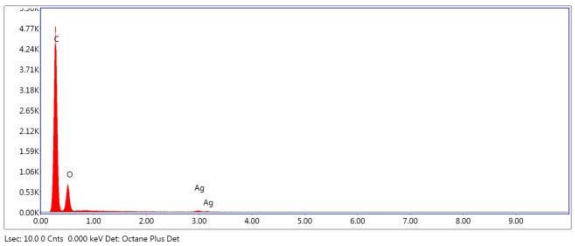

c

Element	Weight %	Atomic %
C K	69.78	75.65
O K	29.87	24.31
AgL	0.35	0.04

d

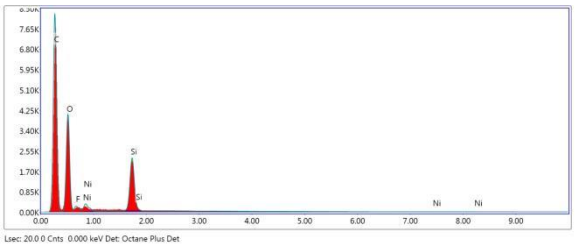

e

Element	Weight %	Atomic %
C K	53.99	62.73
O K	38.47	33.56
F K	2.27	1.66
NiL	2.20	0.52
SiK	3.07	1.52

f

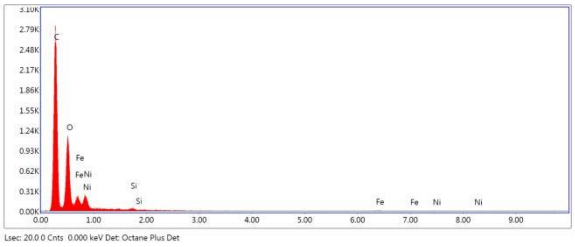

g

Element	Weight %	Atomic %
C K	56.13	63.15
O K	43.48	36.73
SiK	0.11	0.05
FeK	0.13	0.03
NiK	0.16	0.04

h

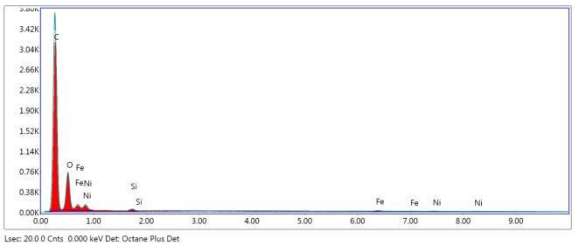

i

Element	Weight %	Atomic %
C K	66.29	74.75
O K	28.20	23.87
FeL	5.17	1.25
SiK	0.16	0.08
NiK	0.19	0.04

j

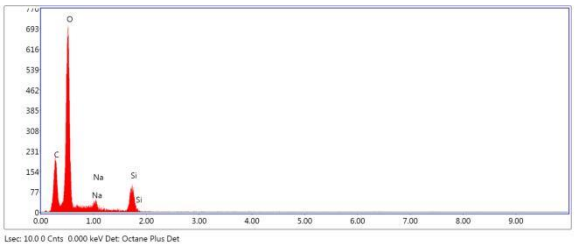

k

Element	Weight %	Atomic %
C K	28.94	36.09
O K	62.91	58.89
NaK	5.66	3.68
SiK	2.50	1.33

l

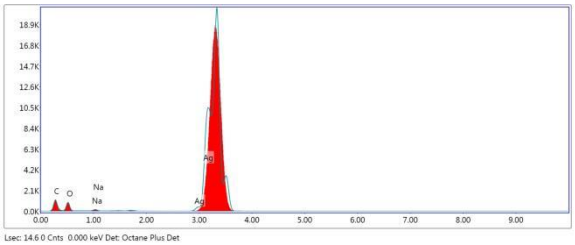

m

Element	Weight %	Atomic %
C K	37.33	47.91
O K	49.98	48.15
NaK	4.04	2.71
AgL	8.65	1.24

n

Figure 2.8. EDX elemental composition on thin films surface: Chit-Oil-AgP-PLD (a), (b), (c), (d); Chit-Oil-GRNT-PLD (e), (f) (i), (j); Chit-AcC-AgP-PLD (k), (l), (m), (n)

The Chit-Oil- AgP thin film elemental composition (Figure 2.8 a-d)analyzed with EDX method denote ablated Ag with an uniform distribution in the thin film (0.03%-0.04% atomic percentage). The thin film obtained from Chit-Oil-GRNT contain Fe, Si, Ni as impurities resulted from the garnet ablation (Figure 2.8 e-j). Although on a spot from an area of the thin film obtained from the Chit-AcC-AgP sample, silver was identified in a large percentage (1.24% in atomic percentages), the fact that it is an isolated value, denotes a large non-uniformity of the composition of the Chit-AcC-AgP layer.

COMSOL numerical simulation was performed for Chit-Oil; and Chit-Oil-AgP laser irradiation. The parameters in the numerical model are the same as in the experiments.

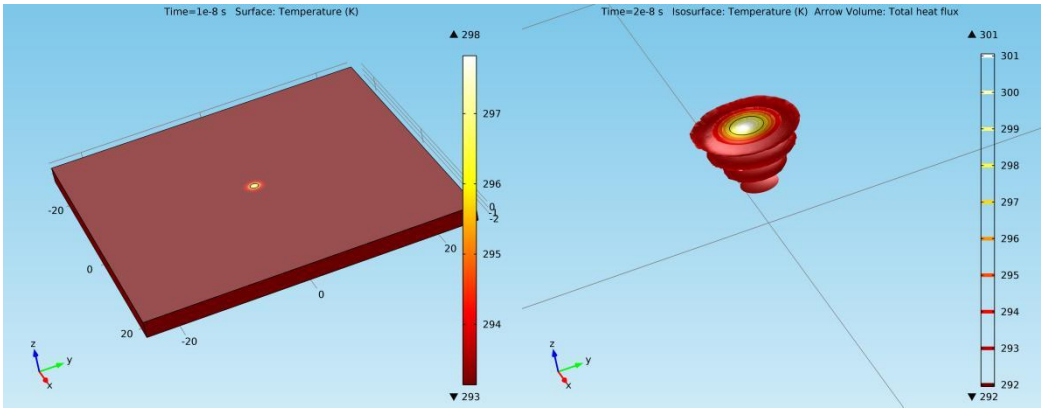

a b

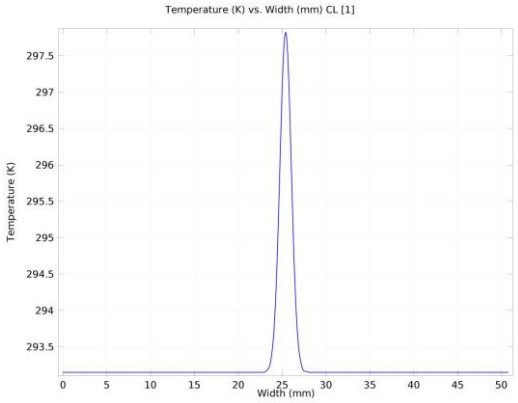

c

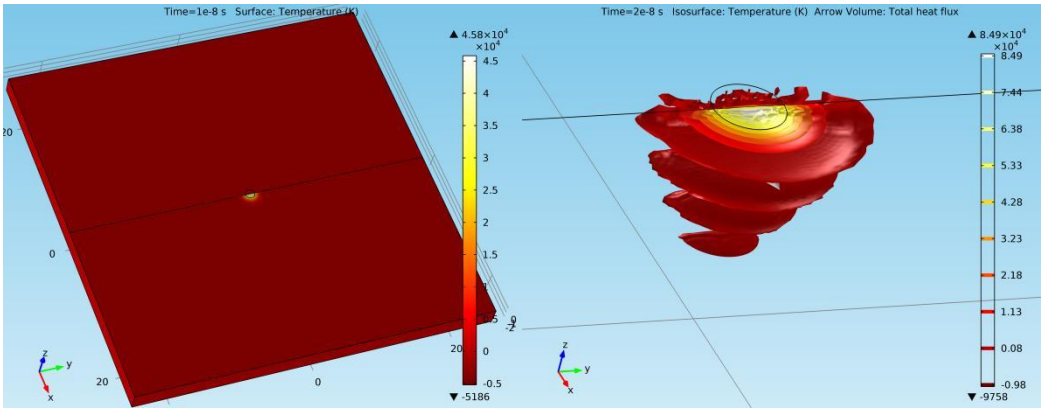

d e

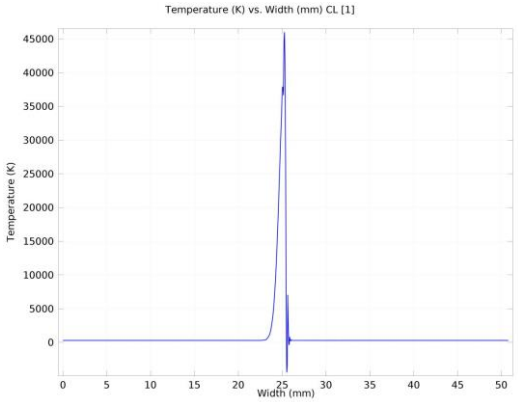

f

Figure 2.9. COMSOL numerical simulation of laser heating at 60 mJ and 650 μm beam radius: Chit-oil 2D surface temperature (a), 3D isosurface (b), 1D surface temperature (c); Chit-oil-AgP 2D surface temperature (d), 3D isosurface (e), 1D surface temperature (f)

The results of the simulation sustain and explain the experiments (Figure 2.9 . The oil, due to its low extinction coefficient, does not absorb the laser beam. In the mixture denoted as Chit-Oil, the particles of chitosan are coated with an oil film which makes them also inactive in the laser irradiation process. When silver particles are placed in a chitosan-oil matrix, the thermal effects are highly increased and plasma threshold is achieved with temperatures of $4.5x10^{-4}$ K.
The experimental results also indicate that the oil behaves as a carrier of silver atoms, ions and clusters, contributing to the uniform dispersion on the support surface. The specific fluid instabilities during laser ablation and deposition [5] are evidenced by the droplets on the surface of Chit-Oil-AgP-PLD.
Difficulties consist in finding a way to handle and transport the Chit-Oil-AgP produced PLD of AgNP in oil

References:

[1] I. Cocean, A. Cocean, C. Postolachi, V. Pohoata, N. Cimpoesu, G. Bulai, F. Iacomi, S. Gurlui, ***Alpha keratin amino acids behvior under high fluence laser interaction. Medical applications***, Applied Surface Science 488 (2019) 418–426, DOI: 10.1016/j.apsusc.2019.05.207

[2] A. Cocean, I. Cocean, N. Cimpoesu, G. Cocean, R. Cimpoesu, C. Postolachi, V. Popescu and S. Gurlui, ***Laser Induced Method to Produce Curcuminoid-Silanol Thin Films for Transdermal Patches Using Irradiation of Turmeric Target***, Appl. Sci. 2021, 11(9), 4030. https://doi.org/10.3390/app11094030

[3] Georgiana Cocean, Alexandru Cocean, Cristina Postolachi, Silvia Garofalide, Georgiana Bulai, Bogdanel Silvestru Munteanu, Nicanor Cimpoesu, Iuliana Cocean and Silviu Gurlui, ***High-Power Laser Deposition of Chitosan Polymers: Medical and Environmental Applications***. Polymers 2022, 14, 1537. https:// doi.org/10.3390/polym14081537

[4] Alexandru Cocean, Iuliana Cocean, Georgiana Cocean, Cristina Postolachi, Daniela Angelica Pricop, Bogdanel Silvestru Munteanu, Nicanor Cimpoesu and Silviu Gurlui, ***Study of Physico-Chemical Interactions during the Production of Silver Citrate Nanocomposites with Hemp Fiber***, Nanomaterials 2021, 11, 2560. https://doi.org/10.3390/nano11102560

[5] A. Cocean, I. Cocean and S. Gurlui, ***INFLUENCE OF THE IMPURITIES TO THE COMPOSITE MATERIALS IN LASER ABLATION PHENOMENA***, U.P.B. Sci. Bull., Series A, Vol. 83, Iss. 3, 2021

[6] Cocean, A.; Cocean, G.; Diaconu, M.; Garofalide, S.; Husanu, F.; Munteanu, B.S.; Cimpoesu, N.; Motrescu, I.; Puiu, I.; Postolachi, C.; Cocean, I. and Gurlui, S. ***Nano-Biocomposite Materials Obtained from Laser Ablation of Hemp Stalks for Medical Applications and Potential Component in New Solar Cells***. Int. J. Mol. Sci. 2023, 24, 3892. https://doi.org/10.3390/ijms24043892

[7] Cocean, G.; Cocean, A.; Garofalide, S.; Pelin, V.; Munteanu, B.S.; Pricop, D.A.; Motrescu, I.; Dimitriu, D.G.; Cocean, I.; Gurlui, S. ***Dual-Pulsed Laser Ablation of Oyster Shell Producing Novel Thin Layers Deposed to Saccharomyces cerevisiae.*** Polymers 2023, 15, 3953. https://doi.org/10.3390/polym15193953